



ARTICLE

# Preparation and Characterization of Biobased Dehydroabietyl Polyethylene Glycol Glycidyl Ether-Grafted Hydroxyethyl Cellulose with High Emulsifying Property

Zhengqing Ding, Quan Yang, Xinyan Yan, Feng Gu, Xujuan Huang\* and Zhaosheng Cai\*

School of Chemical and Chemistry, Yancheng Institute of Technology, Yancheng, 224051, China

\*Corresponding Authors: Xujuan Huang. Email: iamhuangxujuan@163.com; Zhaosheng Cai. Email: jsyc\_czs@163.com

Received: 18 February 2023 Accepted: 20 March 2023 Published: 23 January 2024

## ABSTRACT

Dehydroabietyl polyethylene glycol glycidyl ether-grafted hydroxyethyl cellulose (HEC) polymer surfactant (DA(EO)<sub>5</sub>GE-g-HEC) was prepared using ring-opening polymerization with biobased rosin and hydroxyethyl cellulose as feedstocks. Dehydroabietyl polyethylene glycol glycidyl ether (DA(EO)<sub>5</sub>GE) was formed by condensation of dehydroabietyl alcohol polyoxyethylene ether (Rosin derivative: DA(EO)<sub>5</sub>H) and epichlorohydrin. The grafting degree of DA(EO)<sub>5</sub>GE-g-HEC was manipulated by adjusting the mass ratio of HEC and DA(EO)<sub>5</sub>GE and confirmed by EA. According to the formula, when  $m_{(HEC)}/m_{(DA(EO)_2GE)}$  was 1:1~1:5, the grafting rate of DA(EO)<sub>5</sub>GE in DA(EO)<sub>5</sub>GE-g-HEC varied from 34.43% to 38.33%. The surface activity and foam properties of DA(EO)<sub>5</sub>GE-g-HEC aqueous solution were studied. The results showed that with the increase in grafting rate, the critical micellar concentration (CMC) in aqueous solution changed from 1.28 to 0.96 g/L. The results of the thermogravimetric analysis showed that the temperature range of the main stage of mass loss of DA(EO)<sub>5</sub>GE-g-HEC was 310°C~410°C, and the thermal decomposition processes of the samples with five mass ratios were similar. An oil in water emulsion was prepared by choosing cyclohexane as the oil phase and DA(EO)<sub>5</sub>GE-g-HEC as the emulsifier. The effect of DA(EO)<sub>5</sub>GE-g-HEC mass fraction on emulsion particle size and stability was analyzed. The results suggested that when the oil-water ratio was 8:2 with 0.4% emulsifier, the emulsion droplets were the smallest in terms of particle size and were the most stable. The rheological test results showed that the apparent viscosity decreased with the increase in shear rate and showed a typical elastic gel phenomenon.

## KEYWORDS

Rosin; hydroxyethyl cellulose; surfactant; emulsion; rheological behaviour

## Nomenclature

HEC	Hydroxyethyl cellulose
DA(EO) <sub>5</sub> GE	Dehydroabietyl polyethylene glycol glycidyl ether
DA(EO) <sub>5</sub> H	Dehydroabietyl alcohol polyoxyethylene ether
CMC	Critical micelle concentration
PEG	Polyethylene glycol
DMSO	Dimethyl sulfoxide
DTG	Derivative thermogravimetric



TG            Thermogravimetric  
EA            Elemental analysis

## 1 Introduction

Surfactants are amphiphilic molecules with polar hydrophilic groups and non-polar hydrophobic groups [1,2]. Compared with small molecular surfactants, polymer surfactants have higher molecular weight, in the range of thousands and above [3], along with higher viscosity, which is beneficial to film formation [4], emulsification [5], dispersion [6], thickening [7], flocculation [8] and wetting [9]. At present, people are paying more and more attention on how to use biomass-based renewable feedstocks for new generation green materials to replace the current petrochemical-based products to reduce environmental strain, tackle the issue of energy shortage and eliminate reliance on non-biodegradable resource, which is crucial for the sustainability of our society [10–13]. Cellulose is one of the most abundant natural renewable hydrophilic polymers and is widely used as an emulsifier, stabilizer, and thickener due to the large amount of inherent active hydroxyl groups that make it easy to be chemically modified [14–16]. The current literatures suggest cellulose polymer surfactants have been introduced reasonably frequently. However, the majority of them suffer from drawbacks like having more hydrophilic groups or being difficult to increase surface activity, among others [17]. There are still many problems in the field of bio-based polymers. Designing and synthesizing advanced high-performance bio-based polymers with natural advantages will be a major breakthrough in polymer science [18].

Rosin is a solid resin extracted from pine trees after distillation. Resin acid is the main component in the mixture that accounts for over 90% of its component. Its chemical reactivity lies in the monocarboxylic acid, and unsaturated carbon-carbon double bonds in the hydrogenated phenanthrene ring structure, and the ring structure makes it have high thermal stability [19,20]. When introducing the unique rigid structure of rosin into the cellulose unit chain, rosin shows not only excellent thermodynamic properties [21] but also strong hydrophobicity. It is often used as a hydrophobic agent to make the modified products have hydrophilic and lipophilic groups at the same time [22,23], which creates surface activity. Rosin and its derivatives are widely used in the synthesis and modification of polymer materials, nanocomposites, functional materials, and coating materials [24,25]. For example, Lu et al. designed and synthesized rosin-grafted ethyl cellulose (EC) copolymer (EC-(g-DAPE)-g-PLMA) by atom transfer radical polymerization (ATRP) and click chemistry. The results showed that after modification, the hydrophobicity was improved, and the contact angle increased with the increase of rosin content. The contact angle of unmodified EC was 75.2°, while that of cellulose-rosin copolymer film was above 97°. In addition, the hydrogenated phenanthrene ring structure of rosin further improves the thermal stability of the graft copolymer [23]. Yu et al. synthesized a rosin-based polymer (DA-g-P(MMA-co-LMA)) using 2-bromoisobutyrate hydroxyethyl ester as initiator and dehydroabietic acid (DA) as raw material. Due to the introduction of DA, the thermal stability, hydrophobicity, and mechanical properties of DA-g-P(MMA-co-LMA) were improved. The presence of rosin structure increases the contact angle by  $4.6^\circ \pm 0.8^\circ$  [26]. Polyethylene glycol (PEG) is a kind of hydrophilic polymer polyether compound, which is mainly composed of ethylene oxide unit addition polymerization. It can dissolve with a variety of polar organic solvents with the advantages of environmentally friendly, non-toxic, and easy to store and transport. Introducing PEG structure into biological macromolecules can adjust the hydrophilic and lipophilic balance of surfactants, thus broadening its application [27].

Polymer surfactant is also an important emulsifier due to that polymer surfactant can reduce the interfacial tension to stabilize the emulsion [28], and the molecules adsorbed on the oil-water interface tend to form a dense interface film increasing the steric hindrance [29]. Akiyama et al. developed an amphiphilic high molecular weight polymer HHM-HEC (hydrophilic-hydrophobic modified hydroxyethyl

cellulose) as a thickener and then added a small amount of lipophilic surfactant to adjust the hydrophilic-lipophilic balance. Simultaneously reduce the oil/water (O/W) interfacial tension and reduce the particle size of oil droplets to build a stable O/W emulsion system [30]. Jiang et al. proposed a synergistic composite system of polyvinyl alcohol (HPVA) and cetyltrimethylammonium bromide (CTAB). When  $m_{(HPVA)}/m_{(CTAB)}$  is 7:3, and the total concentration of the system is 3000 mg/L, the spontaneous emulsification system based on HPVA/CTAB mixed surfactant has the best effect, and the emulsion is more stable. The synergistic action of HPVA and CTAB enhances the intermolecular attraction, resulting in greater interfacial membrane strength and delayed demulsification time [31]. The emulsification of polymer surfactants mainly depends on two factors. The first is the surfactant molecules adsorb on the oil-water interface to reduce interfacial tension and thus have surface activity. The second reason is that the surfactant forms a three-dimensional network structure in the aqueous solution, which reduces the collision of oil droplets and enhances the stability of the emulsion. The emulsifying ability is also related to the hydrophilic-lipophilic balance value (HLB) of the surfactant and the adaptability of the oil phase. The higher the fitness, the more stable the emulsion [32]. The emulsifying ability of bio-based polymer surfactants plays an extremely important role in practical applications, especially in oil exploitation, recovery, cosmetics, pharmaceutical, and other industries.

In this study, dehydroabiatic acid was separated from natural biological material disproportionated rosin, and dehydroabiatic alcohol was obtained by chemical conversion. PEG structure was introduced into dehydroabiatic alcohol to change its water solubility while maintaining its natural and biocompatibility [33,34]. DA(EO)<sub>5</sub>H was synthesized by condensation and the addition of dehydroabiatic alcohol and ethylene oxide (EO), and then reacted with epichlorohydrin to synthesize rosin-based active intermediate DA(EO)<sub>5</sub>GE containing epoxy group in the presence of BF<sub>3</sub>-ether. After the ring-opening reaction to hydroxyl groups HEC, hydrophilic-lipophilic groups were introduced into the macromolecular chain, and a series of cellulose-based polymer surfactants (DA(EO)<sub>5</sub>GE-g-HEC) with different grafting ratios were prepared. The role of rosin rigid structure in DA(EO)<sub>5</sub>GE-g-HEC was fully confirmed from the aspects of thermal stability, surface activity, and emulsifying properties. This work introduces a green and economical method to synthesize new amphiphilic polymer surfactants through hydrophobic modification and further optimize the properties of bio-based polymer materials. The results open up a new path for the high-value utilization of green surfactants.

## 2 Experimental Part

### 2.1 Main Instruments and Reagents

Rotary evaporator (RE-2000B, Shanghai Yarong biochemical instrument Factory, China); Electronic analytical balance (AY220, Shimadzu, Japan); Fourier transform Infrared spectrometer (NEXUS 670, Nicolet, USA); Freeze dryer (Scientz-10N, Ningbo Xinzhi Biotechnology Co., Ltd., China); Polarized electron microscope (BM-1000, Nanjing Jiangnan Yongxin Optical Co., Ltd., China). Automatic interface tension instrument (JYW-2000B, Chengde Shipeng testing equipment Co., Ltd., China); High-speed shear dispersion machine (ULTRA-TURRAX, Shanghai Kehuai Instrument Co., Ltd., China); Synchronous thermal analyzer (NETZSCH STA409 PC/PG, NETZSCH, Germany); Rotary rheometer (TA HR10 DISCOVERY, TA instrument Co., Ltd., USA); Element analyzer (Vario EL Cube, Elementar, Germany); Multi-head magnetic mixer (HJ-4A, Jintan Xicheng Xinrui Instrument Factory, China). Heat collector constant temperature heating magnetic agitator (DF-101S, Shanghai Lichen Bangxi Instrument Technology Co., Ltd., China).

Dehydroabietyl polyethylene glycol glycidyl ether, an industrial custom product, was purchased from Linyi Guoli Chemical Co., Ltd., China; Hydroxyethyl cellulose, 2% viscosity: 25–150 mPa.s, purchased from Shanghai Macklin Biotechnology Co., Ltd., China; Dimethyl sulfoxide (DMSO), analytically pure, purchased from Shanghai Aladdin Biotechnology Co., Ltd., China; Ethyl acetate, analytically pure,

purchased from Shanghai Titan Technology Co., Ltd., China; Crystalline tin tetrachloride, analytically pure, purchased from Shanghai Lingfeng Chemical Reagent Co., Ltd., China; BF<sub>3</sub>-ether, analytically pure, purchased from Shanghai Titan Technology Co., Ltd.; Toluene, analytically pure, purchased from Shanghai Lingfeng Chemical Reagent Co., Ltd.; sodium hydroxide, analytically pure, purchased from Shanghai Lingfeng Chemical Reagent Co., Ltd.; epichlorohydrin, analytically pure, purchased from Shanghai Lingfeng Chemical Reagent Co., Ltd.; Cyclohexane, analytically pure, purchased from Shanghai Titan Technology Co., Ltd.; Span 80, analytically pure, purchased from Shanghai Titan Technology Co., Ltd.; Tween 60, analytically pure, purchased from Shanghai Titan Technology Co., Ltd.

## 2.2 Experimental Methods.

### 2.2.1 Preparation of DA(EO)<sub>5</sub>GE

According to the method similar to that in reference [35], the details of the preparation process are as follows: 25 g of dehydroabietyl polyoxyethylene ether was dissolved in 50 mL solvent toluene, stirred until completely dissolved, the metered BF<sub>3</sub>-ether catalyst (DA(EO)<sub>5</sub>H) was added to the reaction bottle, and the stirring and reflux device was installed. The constant pressure drop funnel was used to slowly add epichlorohydrin to the reaction mixture (the molar ratio of DA(EO)<sub>5</sub>H was 3). During the dripping process, the temperature of the material in the reaction bottle always did not exceed 25°C. Stirred for some time after dripping, the temperature was adjusted to 65°C, and the reaction time was controlled at 6.5 h. At the end of the reaction, a dark reddish brown oily viscous liquid was obtained by reduced pressure distillation to a liquid-free form, then a proper amount of toluene was added to the distilled material. At the same time, 40% NaOH solution (molar ratio of dehydroabietyl alcohol was 1) was added to the reaction bottle, stirred at 30°C~40°C for 5 h, then filtered, washed to neutral with supersaturated NaCl aqueous solution, and separated into the oil phase. Finally, the product DA(EO)<sub>5</sub>GE was obtained by drying with anhydrous sodium sulfate and evaporating the solvent toluene under reduced pressure.

### 2.2.2 Preparation of DA(EO)<sub>5</sub>GE-g-HEC

A certain amount of raw material HEC was fully dissolved in anhydrous DMSO and poured into the reaction bottle of 100 mL. The corresponding proportion of DA(EO)<sub>5</sub>GE was added to the HEC solution, the temperature of the mixed solution was raised to 60°C by uniform stirring, and the mixed solution of 0.05 g SnCl<sub>4</sub> and 10 mL anhydrous DMSO was slowly added as the catalyst. The time began after the end of dripping, and the reaction was kept for 0.5 h. At the end of the reaction, ethyl acetate was added to precipitate the white solid product, filtered, the solid product was redispersed in distilled water, dialyzed for 24 h, vacuum distillation, and freeze, drying, the solid product of hydroxyethyl cellulose grafted with dehydroabietyl polyethylene glycol glycidyl ether (DA(EO)<sub>5</sub>GE-g-HEC) was prepared, and the material ratio  $m_{(DA(EO)_5GE)}/m_{(HEC)}$  changed from 1 to 5. Five kinds of rosin-based intermediates with different molecular weights were prepared, and the optimum conditions were determined. Fig. 1 shows the synthesis process of rosin-based intermediate DA(EO)<sub>5</sub>GE and DA(EO)<sub>5</sub>GE-g-HEC.

### 2.2.3 Determination of Grafting Rate of DA(EO)<sub>5</sub>GE-g-HEC

The content of carbon (C) and hydrogen (H) in HEC and its product DA(EO)<sub>5</sub>GE-g-HEC were determined, and the grafting rate of the product was calculated and analyzed according to formula (1).

$$A\% = \frac{C_{(DA(EO)_2GE-g-HEC)} - C_{(HEC)}}{(C_{(DA(EO)_2GE)} - C_{(HEC)})} \times 100\% \quad (1)$$

In the formula,  $A\%$  is the grafting rate of the graft product DA(EO)<sub>5</sub>GE-g-HEC,  $C_{(DA(EO)_2GE-g-HEC)}$  is the C content in DA(EO)<sub>5</sub>GE-g-HEC,  $C_{(DA(EO)_2GE)}$  is the C content in DA(EO)<sub>5</sub>GE, and  $C_{(HEC)}$  is the C content in HEC [36].

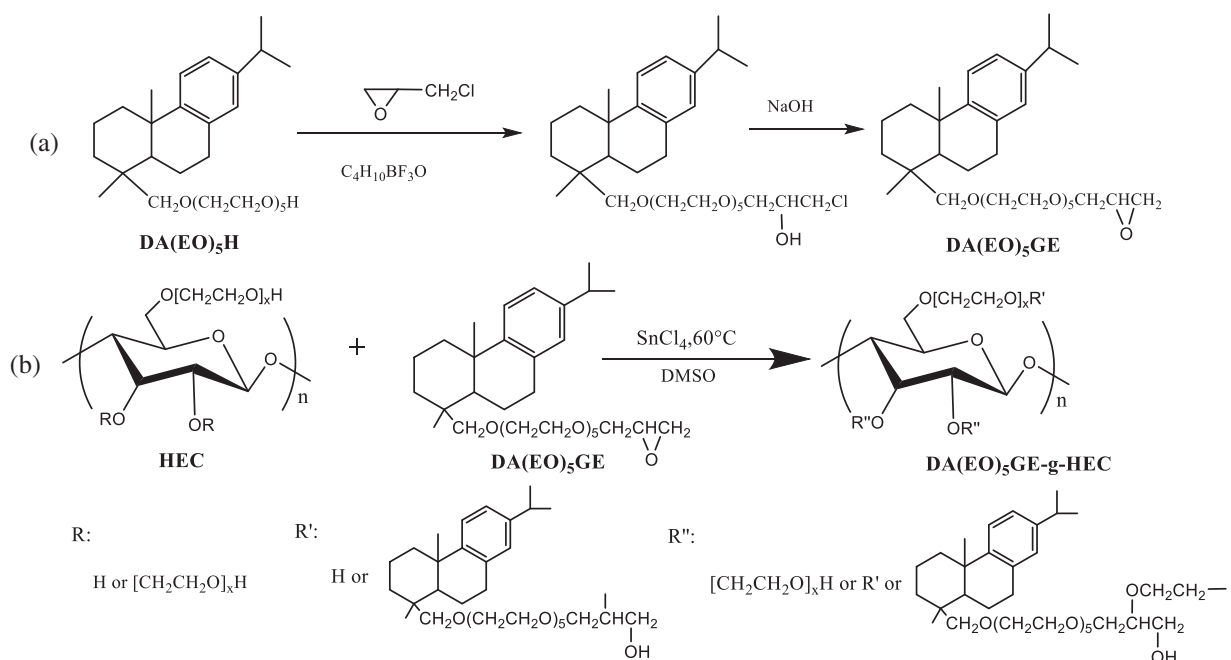


**Figure 1:** Synthesis routes of DA(EO)<sub>5</sub>GE (a) and DA(EO)<sub>5</sub>GE-g-HEC (b)

#### 2.2.4 Structural Characterization

The surface functional groups of raw materials and grafted products were characterized by using the Fourier transform infrared spectroscopy instrument of model NEXUS670. The resolution was 4 cm<sup>-1</sup>, the wavenumber scanning range was 4000~450 cm<sup>-1</sup>, and the scanning times were 32 times. The characteristic functional groups were found out, and the products were synthesized successfully or not.

#### 2.2.5 Determination of HLB Value of DA(EO)<sub>5</sub>GE-g-HEC

Nonionic surfactants are composed of a hydrophilic head group and a hydrophobic tail group, and the balance between the two groups is called hydrophilic-lipophilic balance value (HLB). Two kinds of emulsifiers with different HLB values (Tween 60, HLB = 14.9) and Span 80 (HLB = 4.7) were selected to prepare emulsions. The mass of a single emulsifier was calculated according to Formula (2). A series of mixed emulsifiers with different HLB values were prepared, adding 0.1% DA(GE)<sub>5</sub>GE-g-HEC aqueous solution and stirring by an external force. The HLB value of the emulsion with the best stability is the HLB value of the surfactant DA(GE)<sub>5</sub>GE-g-HEC.

$$HLB_m = HLB_T \times T\% + HLB_S \times S\% \quad (2)$$

In the formula,  $HLB_T$  and  $HLB_S$  are the HLB values of Tween 60 and Span 80,  $T\%$  and  $S\%$  are the mass fraction of Tween 60 and Span 80, respectively, and  $HLB_m$  is the HLB value of mixed emulsifiers [37,38].

#### 2.2.6 Thermogravimetric Analysis of DA(EO)<sub>5</sub>GE-g-HEC

The thermal stability of DA(EO)<sub>5</sub>GE-g-HEC was tested by NETZSCH STA409 PC/PG synchronous thermal analyzer. The test condition under N<sub>2</sub> atmosphere with a temperature range of 40°C~600°C at a heating rate of 10°C/min.

#### 2.2.7 Surface Activity of DA(EO)<sub>5</sub>GE-g-HEC

The aqueous solution of surfactant DA(EO)<sub>5</sub>GE-g-HEC with a mass fraction of 0.4% was prepared, and a series of solutions with different mass fraction were obtained by the double dilution method. The surface

tension ( $\gamma$ ) of DA(EO)<sub>5</sub>GE-g-HEC aqueous solution was measured using the hanging ring method by JYW-2000B automatic interface tensiometer. Deionized water was used to calibrate before the test. Each mass fraction was tested at least three times in the order from low mass fraction to high mass fraction, and the average value was taken. Draw the curve of the relationship between surface tension and concentration, and analyze and evaluate its surface performance.

### 2.2.8 Foam Properties of DA(EO)<sub>5</sub>GE-g-HEC

The aqueous solution of DA(EO)<sub>5</sub>GE-g-HEC (I~V) surfactant with 40 mL concentration of 1 g/L was measured in the 100 mL plug measuring cylinder. The solution height was 72 mm, the solution was shaken repeatedly, the initial foam height was measured immediately and recorded, and the foam height was read at the end of 5 min. Each sample was tested at least three times, and the average value was recorded [39].

### 2.2.9 Emulsifying Property of DA(EO)<sub>5</sub>GE-g-HEC

First, the aqueous solution of surfactant DA(EO)<sub>5</sub>GE-g-HEC with a mass fraction of 0.4% was prepared. At room temperature, the volume ratio of oil to water was changed successively (4:6, 5:5, 6:4, 7:3, 8:2), and the surfactant mass fraction (0.02%, 0.05%, 0.1%, 0.2%, 0.4%) was used to prepare the emulsion. A high-speed shear disperser emulsified the mixed solution in the glass sample bottle, the rotational speed was 12000 r/min, the effective working time was 5 min, intermittent 20 s, and the effect of surfactant mass fraction on the static stability of the emulsion was analyzed and discussed.

The type of emulsion was identified by the dilution method and staining method. The emulsions stabilized by DA(EO)<sub>5</sub>GE-g-HEC were dropped into the water and oil phases, respectively, and the dispersion of the emulsion droplets in them was observed. When the emulsion droplets can be well dispersed in the water phase but cannot be dispersed in the oil phase, the emulsion is an oil-in-water (O/W) emulsion. Otherwise, it was a water-in-oil type (W/O) emulsion. The emulsion droplets were spread flat on the glass slides and dyed with the oil-soluble dye Sudan red and water-soluble dye methylene blue, respectively. The micro-morphology of the emulsion was observed by polarizing electron microscope. When the emulsion was dyed with water-soluble dyes, the external phase was dyed as a whole and showed blue, which was an O/W emulsion. If only the inner phase was dyed, the liquid beads would be blue and were W/O emulsion. When oil-soluble dyes were used, on the contrary, they were red.

### 2.2.10 Rheological Properties of DA(EO)<sub>5</sub>GE-g-HEC Stabilized Emulsion

The rheological test of DA(EO)<sub>5</sub>GE-g-HEC stabilized emulsion was carried out by using a model TA HR10 DISCOVERY rotary rheometer, and the relationship between apparent viscosity and shear stress of different mass fraction emulsion with the shear rate was obtained by steady state test, and the steady state rheological test conditions were as follows: plate with diameter 44 mm, test temperature 25°C, the shear rate range 0.01~1000 s<sup>-1</sup>. Through viscoelastic region scanning, the strain scanning range of 0.01%~1000% was set, the appropriate strain value was determined for the full frequency scanning test, and the emulsion was scanned by vibrating shear. The dynamic viscoelastic test conditions were as follows: a flat plate measuring element with a diameter of 44 mm, a test temperature of 25°C, a fixed scanning frequency  $f$  of 1 Hz, and an angular frequency of 0.01~100 rad/s.

## 3 Results and Discussion

### 3.1 Determination Result and Analysis of Graft Rate

The effect of the mass ratio of HEC to DA(EO)<sub>5</sub>GE ( $m_{\text{HEC}}:m_{\text{DA(EO)}_5\text{GE-g-HEC}}$ ) on the grafting rate of the product is shown in Table 1. The results in the table show that as  $m_{\text{DA(EO)}_5\text{GE}}/m_{\text{HEC}}$  grows, the carbon content of the product structure gradually rises, and the grafting rate rises in lockstep. The ring-opening reaction is more fully completed, and more rosin structure is added to the HEC sugar chain when the amount of DA(EO)<sub>5</sub>GE is increased. However, when  $m_{\text{DA(EO)}_5\text{GE}}/m_{\text{HEC}}$  reaches 4, the grafting rate does not increase significantly with the increase of rosin content.

**Table 1:** Analysis and results of DA(EO)<sub>5</sub>GE-g-HEC elements

The sample	m <sub>(HEC)</sub> :m <sub>(DA(EO)<sub>5</sub>GE)</sub>	C%	H%	Rate of grafting A%
DA(EO) <sub>5</sub> GE-g-HEC I	1.0:1.0	49.65	6.58	34.43
DA(EO) <sub>5</sub> GE-g-HEC II	1.0:2.0	49.98	6.64	35.47
DA(EO) <sub>5</sub> GE-g-HEC III	1.0:3.0	50.24	6.63	36.29
DA(EO) <sub>5</sub> GE-g-HEC IV	1.0:4.0	50.82	6.47	38.11
DA(EO) <sub>5</sub> GE-g-HEC V	1.0:5.0	50.89	6.69	38.33

### 3.2 Structural Characterization

The infrared structure comparison of DA(EO)<sub>5</sub>H and DA(EO)<sub>5</sub>GE is shown in Fig. 2a. It can be seen from Fig. 2a that in the FT-IR spectrum of DA(EO)<sub>5</sub>H, there is a characteristic absorption peak of alcohol hydroxyl groups at 3486 cm<sup>-1</sup> and a characteristic absorption peak of stretching vibration of C-O in polyethylene glycol structure at 1109 cm<sup>-1</sup>, while in the FT-IR of the product DA(EO)<sub>5</sub>GE, the characteristic absorption peak of alcohol hydroxyl groups disappears obviously, and the C-O-C stretching vibration absorption peak reflecting the ether structure appears at 1251, 910, and 839 cm<sup>-1</sup>. The infrared structure spectrum of DA(EO)<sub>5</sub>GE-g-HEC is shown in Fig. 2b. Compared with HEC and DA(EO)<sub>5</sub>GE, the FT-IR of DA(EO)<sub>5</sub>GE-g-HEC shows O-H stretching vibration absorption peak at about 3426 cm<sup>-1</sup>, methyl stretching vibration absorption peak at 2923 cm<sup>-1</sup>, and benzene ring skeleton stretching vibration absorption peak at 1627 cm<sup>-1</sup>. There are stretching vibration absorption peaks at 1064 cm<sup>-1</sup> and strong stretching vibration absorption peaks at 891 cm<sup>-1</sup>. The existence and change of these peaks indicate that HEC and DA(EO)<sub>5</sub>GE have been grafted successfully.

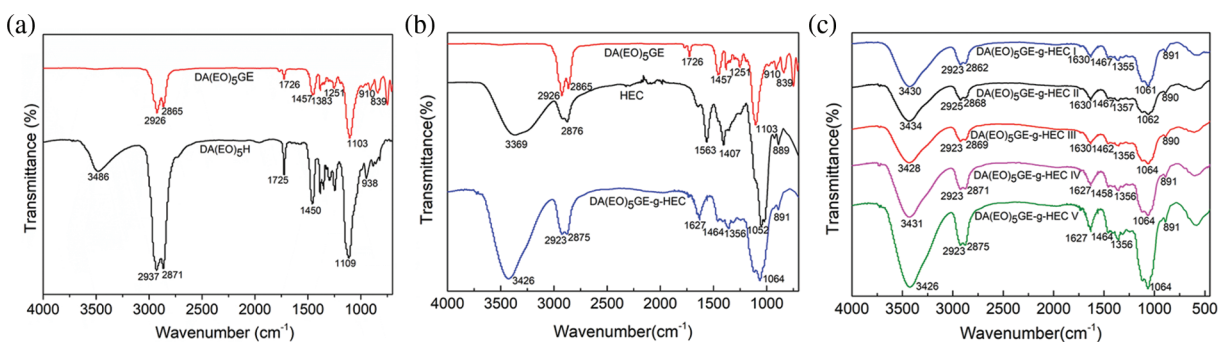


**Figure 2:** FT-IR comparison of DA(EO)<sub>5</sub>H and DA(EO)<sub>5</sub>GE (a); DA(EO)<sub>5</sub>GE-g-HEC and raw material FT-IR (b); FT-IR comparison of DA(EO)<sub>5</sub>GE-g-HEC (I~V) at different grafting degrees (c)

The infrared structure comparison spectra of DA(EO)<sub>5</sub>GE-g-HEC with different grafting degrees are shown in Fig. 2c. It can be known that the stretching vibration of the C-H bond in CH<sub>3</sub> and CH<sub>2</sub> corresponds to around 2860 and 2920 cm<sup>-1</sup>. The intensity of the absorption peak is enhanced, and the intensity of the absorption peak of C-H bending vibration corresponding to 1350~1390 cm<sup>-1</sup> and 1450~1490 cm<sup>-1</sup> is enhanced. In addition, the intensity of the absorption peak reflecting the structure of the benzene ring near 1600 cm<sup>-1</sup> is also enhanced. The intensity change of these peaks is due to the introduction of a more hydrogenated phenanthrene ring and polyoxyethylene chain structure so that the ring-opening reaction is more sufficient, and hydroxyl groups have more opportunities to attack epoxy groups.

### 3.3 Analysis of TG and DTG Determination of DA(EO)<sub>5</sub>GE-g-HEC

The thermal stability and degradability of DA(EO)<sub>5</sub>GE-g-HEC are shown in Figs. 3a and 3b. The DA(EO)<sub>5</sub>GE-g-HEC samples present similar thermal stability and begin to decompose near 290°C. When the temperature reaches 360°C, the components decompose completely. Compared with the raw material HEC, DA(EO)<sub>5</sub>GE-g-HEC, the initial thermal weight loss temperature is increased by 60°C, indicating that the introduction of rosin structure can delay the thermal degradation of HEC to some extent. However, the ash content of HEC remains at 33% after complete decomposition. The DTG curve shows that the sample shows a specific decomposition peak at 270°C~360°C, which is mainly divided into three thermal decomposition stages. The first stage is before 270°C, which is mainly related to the residual water in the sample. The temperature range of the second stage is 270°C~360°C, which is mainly the decomposition of organic compounds. After the third stage, the quality of the sample gradually reaches a constant, and the thermal degradation is complete. The maximum weight loss rate of HEC appears at 275°C, and the maximum weight loss rate of the DA(EO)<sub>5</sub>GE-g-HEC sample appears at 310°C. The temperature of the maximum weight loss rate increases by 35°C, which indicate that the thermal stability of the product is significantly enhanced after successful grafting.

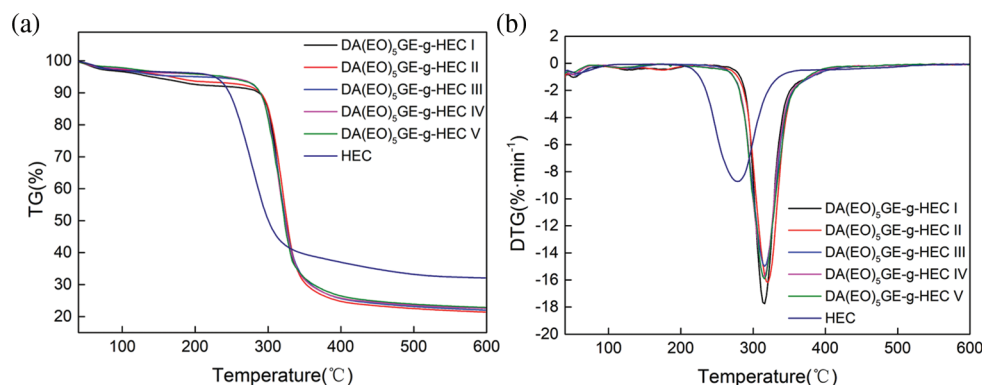


**Figure 3:** Graphs of TG (a) and DTG (b) of HEC and DA(EO)<sub>5</sub>GE-g-HEC

### 3.4 Surface Activity and Foam Properties of DA(EO)<sub>5</sub>GE-g-HEC

The curves in Fig. 4 and the data in Table 2 show that the increase in grafting ratio can significantly improve the surface activity, foaming ability, and foam stability of surfactant DA(EO)<sub>5</sub>GE-g-HEC. The surface tension of DA(EO)<sub>5</sub>GE-g-HEC decreases with the increase of the concentration of the aqueous solution and begins to stabilize when it reaches a certain inflection point. This is mainly attributed to the hydrophobic rigid structure of hydrogenated phenylic rings and hydrophilic HEC sugar chains in the molecular structure of surfactants. When the concentration increases, the molecules are adsorbed on the liquid-gas interface. When the concentration is high enough, the adsorption points on the liquid-gas interface are completely covered [40]. The data analysis in Table 2 shows that the increase of hydrophobic chains in the hydroxyl groups of HEC can give it a better ability to reduce surface tension. When the content of DA(EO)<sub>5</sub>GE increases, the CMC value decreases, indicating that the introduction of a more rigid phenanthrene hydrogen ring structure of rosin can enhance the hydrophobic effect and improve the surface activity of DA(EO)<sub>5</sub>GE-g-HEC. DA(EO)<sub>5</sub>GE-g-HEC also improved foaming and bubble stability due to the decrease of liquid-gas interfacial tension, the easier aggregation of micelles, the adsorption of molecules into films, and the increase of foam elasticity and stability [41].

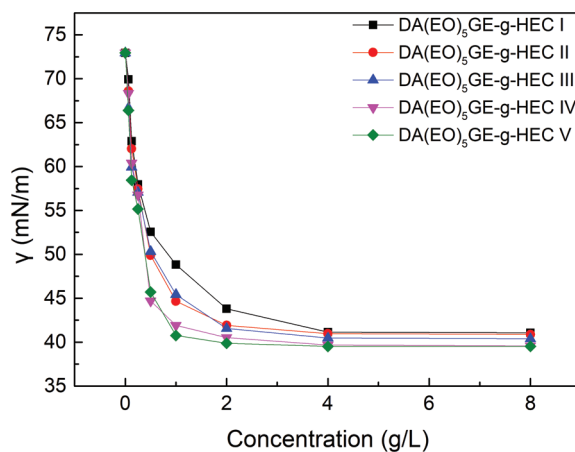


**Figure 4:** Surface tension curves corresponding to different concentrations of DA(EO)<sub>5</sub>GE-g-HEC

**Table 2:** Analysis of surface tension and FP value of DA(HEC)<sub>5</sub>GE-g-HEC aqueous solution under different  $m_{\text{HEC}}/m_{\text{DA(EO)}_5\text{GE}}$  conditions

Sample	CMC (g/L)	$\gamma_{\text{CMC}}$ (mN/m)	$\gamma_{\text{min}}$ (mN/m)	HLB value	FP (mm, $H_0/H_{5\text{min}}$ )
HEC	>5	54.7	—	—	—
DA(EO) <sub>5</sub> GE-g-HEC I	1.28	43.3	41.1	9~10	89.7/2.7
DA(EO) <sub>5</sub> GE-g-HEC II	1.06	41.8	40.9	9~10	94.0/5.7
DA(EO) <sub>5</sub> GE-g-HEC III	1.18	41.4	40.4	9~10	98.0/8.7
DA(EO) <sub>5</sub> GE-g-HEC IV	0.98	39.9	39.6	9~10	106.3/11.7
DA(EO) <sub>5</sub> GE-g-HEC V	0.96	39.8	39.5	9~10	111.0/15.0

### 3.5 Emulsifying Property of DA(EO)<sub>5</sub>GE-g-HEC

The emulsion type is determined to be O/W emulsion by dilution method (Fig. 5a) and dyeing method (Figs. 5b and 5c) [42]. As shown in Fig. 5a, the emulsion droplets stabilized by DA(EO)<sub>5</sub>GE-g-HEC are added to deionized water and oil phase cyclohexane respectively. The emulsion droplets can be uniformly dispersed in water but not in cyclohexane, so it can be verified that the type of emulsion stabilized by DA(EO)<sub>5</sub>GE-g-HEC is O/W type. Figs. 5b and 5c show that the emulsion droplets were dyed with the oil-soluble dye Sudan red and water-soluble dye methylene blue, respectively. It can be observed under the microscope that the outer phase is colored by water-soluble dye and the inner phase is colored by oil-soluble dye, so it can be judged that the type of emulsion stabilized by DA(EO)<sub>5</sub>GE-g-HEC is O/W type.

The effects of O/W volume ratio (4:6, 5:5, 6:4, 7:3, 8:2) and surfactant mass fraction (0.02%, 0.05%, 0.1%, 0.2%, 0.4%) on the static stability of the emulsion were studied. The positive diagram of stable emulsion for 30 days under different oil-water volume ratios is shown in Fig. 5d. When the oil-water volume ratio is 8:2, there is still no delamination for more than one month, and the oil-water phase is completely emulsified, while obvious oil-water separation occurs in other proportions. 8:2 is the best stability ratio. The positive and inverted diagrams of stabilized emulsions with different mass fractions of surfactant DA(EO)<sub>5</sub>GE-g-HEC are shown in Figs. 5e and 5f. The static time is 30 days, the oil-water

volume ratio is 8:2, and the oil phase used in the emulsion is cyclohexane. It can be seen from the diagram that when the emulsion is stable for one month, and the mass fraction is 0.02%, the emulsion is no longer stable and shows oil-water separation. When the mass fraction is 0.05%, 0.1%, 0.2%, and 0.4%, the system's surfactant can play a sufficient stabilizing effect, and the oil-water phase is completely emulsified, and the emulsion is not delaminated. As can be seen from the emulsion inverted diagram, after one month of stabilization, the emulsion will not flow when the mass fraction is 0.4%, and when the mass fraction is 0.02% to 0.1%, the emulsion has fluidity, indicating that the viscosity of the emulsion increases with the increase of emulsifier mass fraction. The emulsion shows a gel-like state at high mass fraction, which can play a better emulsifying role. To sum up, hydrophobically modified HEC can stabilize O/W emulsion without adding any dispersant, and DA(EO)<sub>5</sub>GE-g-HEC molecules accumulate at the oil-water interface, forming a mechanical barrier to avoid droplet collision leading to demulsification [43].

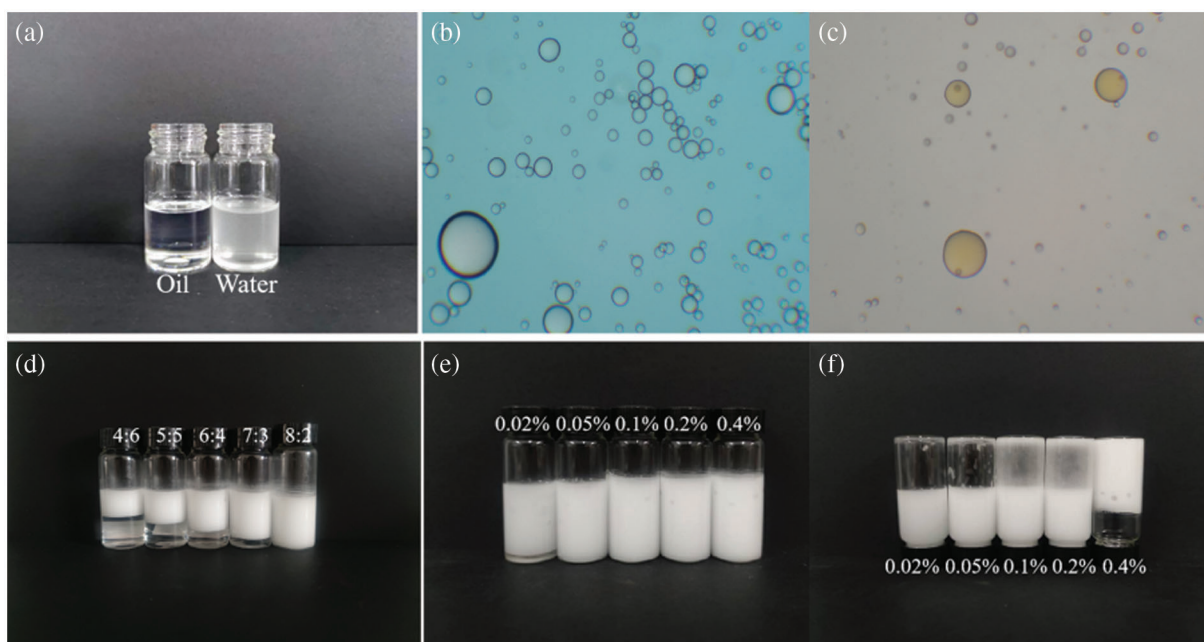


**Figure 5:** DA(EO)<sub>5</sub>GE-g-HEC stabilized emulsion droplet dispersion diagram in cyclohexane and deionized water (a); DA(EO)<sub>5</sub>GE-g-HEC stabilized emulsion stained with methylene blue (b) and Sudan red (c), respectively; DA(EO)<sub>5</sub>GE-g-HEC stabilized emulsion with different oil-water volume ratio for 30 days (d). Positive (e) and inverted (f) diagrams of DA(EO)<sub>5</sub>GE-g-HEC stabilized emulsions standing for 30 days at different mass fraction

As shown in Fig. 6, the microscopic morphology of the emulsion stabilized by surfactant DA(EO)<sub>5</sub>GE-g-HEC shows that the particle size of the emulsion decreases gradually as the mass fraction increases from 0.05% to 0.4%. When the mass fraction of DA(EO)<sub>5</sub>GE-g-HEC is 0.4%, the particle size of the emulsion is smaller and relatively aggregated. This is because, under the condition of high mass fraction, more DA(EO)<sub>5</sub>GE-g-HEC particles are adsorbed on the oil-water interface, forming a higher interfacial film area, thus reducing the particle size of the emulsion and making the emulsion more stable [44,45].

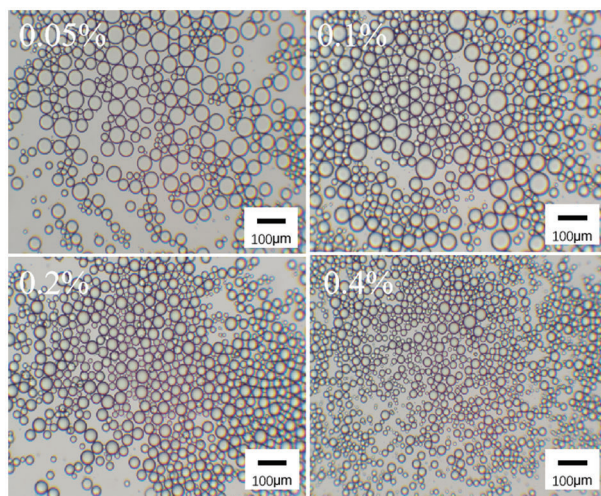


**Figure 6:** Microscopic morphology of DA(EO)<sub>5</sub>GE-g-HEC stabilized emulsion at different mass fraction

### 3.6 Rheological Properties of DA(EO)<sub>5</sub>GE-g-HEC Stabilized Emulsion

The relationship between emulsion stabilization mechanism and rheology is complex and intimate [46]. The rheological properties of emulsions stabilized by DA(EO)<sub>5</sub>GE-g-HEC with different mass fraction (0.05%, 0.1%, 0.2%, 0.4%) were analyzed and discussed. The oil phase used in the tested emulsion was cyclohexane, and the oil-water volume ratio was 8:2. Fig. 7 shows the steady-state rheological test diagram of the emulsion stabilized by DA(EO)<sub>5</sub>GE-g-HEC with different mass fraction, and the change in apparent viscosity is closely related to the shear rate and surfactant mass fraction. When the shear rate is 0.01~1 s<sup>-1</sup>, the apparent viscosity decreases sharply, and the apparent viscosity decreases with the increase of the shear rate, showing the phenomenon of shear thinning, showing pseudoplastic fluid behavior. The higher the mass fraction is, the greater the initial apparent viscosity is, and the more obvious the downward trend is. When the mass fraction is 0.4%, the viscosity is the highest, and the shear thinning is the most obvious; the shear stress increases with the increase of shear rate, and the increase is the largest when the mass fraction of DA(EO)<sub>5</sub>GE-g-HEC is 0.4%. This is due to the increase of the mass fraction of DA(EO)<sub>5</sub>GE-g-HEC in the emulsion, the increase of hydroxyl content to form hydrogen bonding, and the enhancement of the network structure, while the increase of shear rate and the increase of gravitation between the dispersed phases make the structure destroyed.

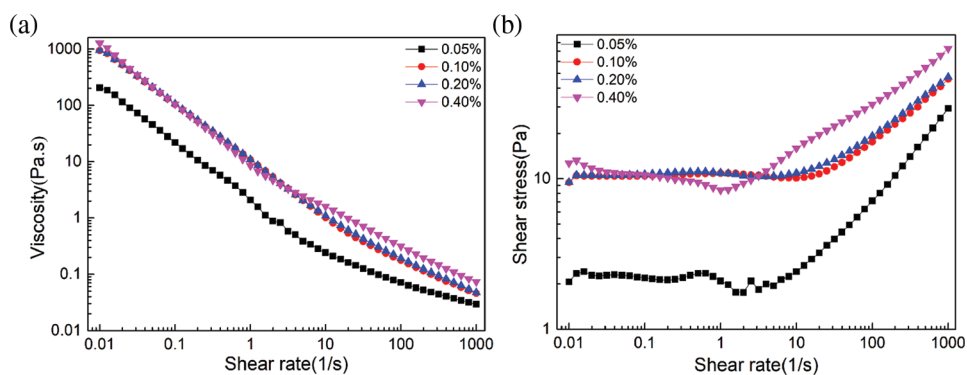


**Figure 7:** Stable emulsions with different mass fraction of DA(EO)<sub>5</sub>GE-g-HEC: (a) the relationship between apparent viscosity and shear rate; (b) the relationship between shear stress and shear rate

As can be seen from Fig. 8, the storage modulus ( $G'$ ) and loss modulus ( $G''$ ) of the emulsion stabilized by the different mass fraction of DA(EO)<sub>5</sub>GE-g-HEC is stable in the strain range of 0.1%~1%. Therefore the value is kept at 0.5% for full-frequency scanning. In Figs. 9a and 9b, both  $G'$  and  $G''$  increase with an increase in the mass fraction of emulsifier DA(EO)<sub>5</sub>GE-g-HEC, and with an increase in frequency; a higher  $G'$  value means that the microstructure of the emulsion maintains strong mechanical stability [47]; it is shown in the figure that at the same mass fraction,  $G'$  and  $G''$  exhibit a typical elastomeric gel phenomenon. In Fig. 9c, when the mass fraction of DA(EO)<sub>5</sub>GE-g-HEC is 0.05%, the loss factor is the largest, while when the mass fraction is 0.1%, the loss factor is the smallest, the viscoelasticity is the strongest, and the gel property is the most obvious; it can be seen that the higher the mass fraction, the better. When the loss factor  $\tan \delta$  is between 0.1 and 1, the elasticity of the sample is higher than that of viscoelasticity.

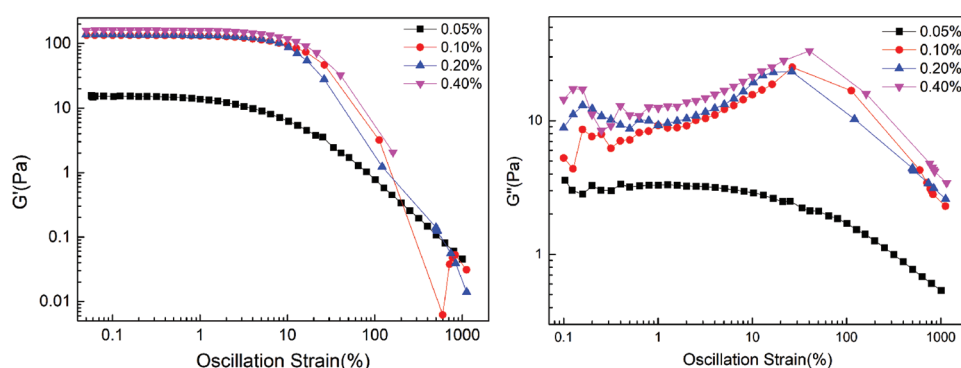


**Figure 8:** Linear viscoelastic strain scanning of emulsions stabilized by DA(EO)<sub>5</sub>GE-g-HEC with different mass fraction

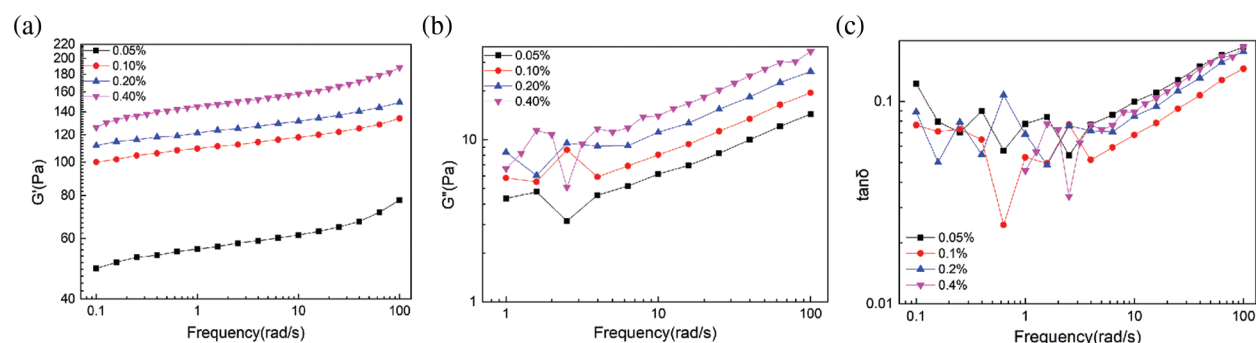


**Figure 9:** Stable emulsions with different mass fraction of DA(EO)<sub>5</sub>GE-g-HEC: (a) relationship between storage modulus and frequency; (b) relationship between loss modulus and frequency; (c) relationship between loss factor and frequency

#### 4 Conclusion

The structure of DA(EO)<sub>5</sub>GE and DA(EO)<sub>5</sub>GE-g-HEC was characterized by FT-IR and elemental analysis, indicating that the hydrophobic structure of rosin was successfully introduced into the HEC unit chain. With the increase of DA(EO)<sub>5</sub>GE content, the grafting rate changed from 34.43% to 38.33%. The thermal stability of DA(EO)<sub>5</sub>GE-g-HEC with different grafting rates is similar. Compared with HEC, the TG and DTG of DA(EO)<sub>5</sub>GE-g-HEC have been significantly improved. The surface properties of DA

(EO)<sub>5</sub>GE-g-HEC showed that the surface tension varied from 43.32 to 39.81 mN/m, and the CMC value also varied from 1.28 to 0.96 g/L with the introduction of the hydrophenylic structure of rosin, and it also had certain foaming and foaming stability. With the increase of the mass fraction of DA(EO)<sub>5</sub>GE-g-HEC in the cyclohexane-water emulsion system, the stability of the emulsion was enhanced; when the volume ratio of oil to water was 8:2 and the mass fraction was 0.4%, the stability of the emulsion could last for more than 60 days, and there was no oil-water separation. The rheological test results showed that the apparent viscosity of the emulsion increases with the increase of the mass fraction of DA(EO)<sub>5</sub>GE-g-HEC. When the mass fraction was 0.05%, the viscosity was lower, and  $G'$  was always greater than  $G''$ , showing good elasticity. This work provides a green and economical method to synthesize amphiphilic polymer surfactants and broaden the application field of biobased rosin.

**Funding Statement:** This research was supported by the National Natural Science Foundation of China (31901257 and 32071706) and School-Level Research Projects of the Yancheng Institute of Technology (xjr2019008).

**Conflicts of Interest:** The authors declare that they have no conflicts of interest to report regarding the present study.

## References

1. Bhardwaj, P., Kamil, M., Panda, M. (2018). Surfactant-polymer interaction: Effect of hydroxypropylmethyl cellulose on the surface and solution properties of gemini surfactants. *Colloid and Polymer Science*, 296(11), 1879–1889.
2. Yang, J., Pal, R. (2020). Investigation of surfactant-polymer interactions using rheology and surface tension measurements. *Polymers*, 12(10), 2302.
3. Bhardwaj, P., Kamil, M., Panda, M. (2019). Salt effect on the solution properties of cationic gemini/conventional surfactants in the presence of the nonionic polymer hydroxypropyl methyl cellulose. *Journal of Surfactants and Detergents*, 22(6), 1279–1288.
4. Tran, B. N., Bhattacharyya, S., Yao, Y., Agarwal, V., Zetterlund, P. B. (2021). *In situ* surfactant effects on polymer/reduced graphene oxide nanocomposite films: Implications for coating and biomedical applications. *ACS Applied Nano Materials*, 4(11), 12461–12471.
5. Zhao, H., Kang, W. L., Yang, H. B., Huang, Z. T., Zhou, B. B. et al. (2021). Emulsification and stabilization mechanism of crude oil emulsion by surfactant synergistic amphiphilic polymer system. *Colloids and Surfaces A: Physicochemical and Engineering Aspects*, 609(1–2), 125726.
6. Asadi-Zaki, N., Mardani, H., Roghani-Mamaqani, H., Shahi, S. (2021). Interparticle cycloaddition reactions for morphology transition of coumarin-functionalized stimuli-responsive polymer nanoparticles prepared by surfactant-free dispersion polymerization. *Polymer*, 228, 123899.
7. Wang, Z. W., Shi, J. N., Liu, R. Q., Zhang, Y., Zhu, Y. F. et al. (2022). A water-soluble polymeric surfactant with thickening water and emulsifying oil simultaneously for heavy oil recovery. *Journal of Molecular Liquids*, 366(3–4), 120293.
8. Hill, C., Abdullahi, W., Crossman, M., Griffiths, P. C. (2022). Using polymer-surfactant charge ratio to control synergistic flocculation of anionic particulate dispersions. *Polymers*, 14(17), 3504.
9. Wan, Q., Zhao, J. Y., Li, H., Li, H., Wang, C. W. et al. (2020). The wetting behavior of three different types of aqueous surfactant solutions on housefly (*Musca domestica*) surfaces. *Society of Chemical Industry*, 76(3), 1085–1093.
10. Wang, H. H., Liu, B., Liu, X. Q., Zhang, J. W., Xian, M. (2008). Synthesis of biobased epoxy and curing agents using rosin and the study of cure reactions. *Green Chemistry*, 10(11), 1190–1196.
11. Zaoui, A., Mahendra, V., Mitchell, G., Cherifi, Z., Harrane, A. et al. (2020). Design, synthesis and thermo-chemical properties of rosin vinyl imidazolium based compounds as potential advanced biocompatible materials. *Waste and Biomass Valorization*, 11(7), 3723–3730.

12. Wang, S. H., Yu, L., Wang, S. S., Zhang, L., Chen, L. et al. (2022). Strong, tough, ionic conductive, and freezing-tolerant all-natural hydrogel enabled by cellulose-bentonite coordination interactions. *Nature Communications*, *13*(1), 3408.
13. Liu, X. X., Yang, X. X., Wang, S. H., Wang, S. B., Wang, Z. P. et al. (2021). Fully bio-based polyhydroxyurethanes with a dynamic network from a terpene derivative and cyclic carbonate functional soybean oil. *ACS Sustainable Chemistry and Engineering*, *9*(11), 4175–4184.
14. Yuan, Z. W., Zhang, J. J., Jiang, A. N., Lv, W. T., Wang, Y. W. et al. (2015). Fabrication of cellulose self-assemblies and high-strength ordered cellulose films. *Carbohydrate Polymers*, *117*(9), 414–421.
15. Liu, W., Liu, K., Du, H. S., Zheng, T., Zhang, N. et al. (2022). Cellulose nanopaper: Fabrication, functionalization, and applications. *Nano-Micro Letters*, *14*(1), 104.
16. Xu, Y. Z., Dai, S. L., Bi, L. W., Jiang, J. X., Zhang, H. B. et al. (2022). Catalyst-free self-healing bio-based vitrimer for a recyclable, reprocessible, and self-adhered carbon fiber reinforced composite. *Chemical Engineering Journal*, *429*(6), 132518.
17. Huerta-Marcial, S. T., Ruiz-Deance, A. L., Mota-Morales, J. D. (2021). Bringing sustainability to macroporous polystyrene: Cellulose nanocrystals as cosurfactant and surface modifier in deep eutectic solvent-based emulsion templating. *ACS Sustainable Chemistry Engineering*, *9*(45), 15109–15116.
18. Su, N., Fang, C. H., Zhou, H., Lu, C. W., Wang, C. P. et al. (2021). Hydrophobic treatment of bamboo with rosin. *Industrial Crops and Products*, *271*, 121507.
19. Liu, K., Du, H. S., Zheng, T., Liu, H. Y., Zhang, M. et al. (2021). Recent advances in cellulose and its derivatives for oilfield applications. *Carbohydrate Polymers*, *259*(2), 117740.
20. Hsieh, C. C., Chen, Y. C. (2020). Synthesis of bio-based polyurethane foam modified with rosin using an environmentally-friendly process. *Journal of Cleaner Production*, *276*(12), 124203.
21. Zeng, Y. N., Li, J. W., Liu, S. X., Yang, B. (2021). Rosin-based epoxy vitrimers with dynamic boronic ester bonds. *Polymers*, *13*(19), 3386.
22. Su, N., Zhou, H., Tang, T., Zhang, S. Q., Yu, Z. X. et al. (2021). Penetration and distribution of rosin along the longitudinal axis of round bamboo culm. *Construction and Building Materials*, *305*(7411), 124781.
23. Lu, C. W., Qiu, Y. L., Guo, X. L., Wang, C. P., Wang, J. F. et al. (2020). Combination of atom transfer radical polymerization and click chemistry toward cellulose-rosin derived UV-absorbent copolymers. *Iranian Polymer Journal*, *29*(11), 975–983.
24. Fu, F., Wang, D., Shen, M. G., Shang, S. B., Song, Z. Q. et al. (2020). Preparation of planar and hydrophobic benzocyclobutene based dielectric material from biorenewable rosin. *Journal of Applied Polymer Science*, *137*(26), 48831.
25. Sun, P. H., Wang, S. H., Huang, Z., Zhang, L., Dong, F. H. et al. (2022). Water-resistant, strong, degradable and recyclable rosin-grafted cellulose composite paper. *Green Chemistry*, *24*(19), 7519–7530.
26. Yu, J., Xu, C. Q., Song, X. L., Lu, C. W., Wang, C. P. et al. (2021). Synthesis and properties of rosin grafted polymers via “grafting from” ATRP: The role of rosin-based initiator. *Industrial Crops and Products*, *168*, 113610.
27. Lin, Y. F., Xie, Z., Zhou, J., Chen, H. H., Shao, W. W. et al. (2019). Effect of exogenous spastin combined with polyethylene glycol on sciatic nerve injury. *Neural Regeneration Research*, *14*(7), 1271–1279.
28. Errezma, M., Mabrouk, A. B., Magnin, A., Dufresnac, A., Bouf, S. (2018). Surfactant-free emulsion Pickering polymerization stabilized by aldehyde-functionalized cellulose nanocrystals. *Carbohydrate Polymers*, *202*, 621–630.
29. Camino, N. A., Sanchez, C. C., Rodríguez Patino, J. M., Pilosof, A. M. R. (2011). Hydroxypropylmethyl cellulose at the oil-water interface. Part I. Bulk behaviour and dynamic adsorption as affected by pH. *Food Hydrocolloids*, *25*(1), 1–11.
30. Akiyama, E., Kashimoto, A., Hotta, H., Kitsuki, T. (2006). Mechanism of oil-in-water emulsification using a water-soluble amphiphilic polymer and lipophilic surfactant. *Journal of Colloid and Interface Science*, *300*(1), 141–148.

31. Jiang, J. T., Kang, X., Wu, H. R., Lu, Y., Li, Z. et al. (2021). Spontaneous emulsification induced by a novel surfactant-polymer compound system and its application to enhance oil recovery. *Journal of Molecular Liquids*, 337, 116399.
32. Wei, Y. S., Xiong, Y. M., Guo, B. M., Yan, H. B. (2020). Study on the influencing factors of the emulsion stability of a polymeric surfactant based on a new emulsification device. *Energies*, 13(18), 4794.
33. Liu, P., Liu, X. M., Saburi, T., Kubota, S., Huang, P. X. et al. (2020). Thermal stability evaluation of resin acids and rosin modified resins. *ACS Omega*, 5(45), 29102–29109.
34. Ummartyotin, S., Manuspiya, H. (2015). A critical review on cellulose: From fundamental to an approach on sensor technology. *Renewable and Sustainable Energy Reviews*, 41, 402–412.
35. Huang, X. J., Ding, Z. Q., Cai, Z. S., Wang, T., Yang, X. X. et al. (2022). Preparation and characterization of hydrogels based on dehydroabietyl polyoxvethvlene glycidyl ether grafted hydroxyethyl chitosans and their capability for loading and controlled release of chloramphenicol. *BioResources*, 17(3), 4331–4346.
36. Huang, X. J., Liu, H., Shang, S. B., Rao, X. P., Song, J. (2015). Preparation and characterization of polymeric surfactants based on epoxidized soybean oil grafted hydroxyethyl cellulose. *ACS Publication*, 63(41), 9062–9068.
37. Reka, K., Roland, N., Laszlo, B. (2017). Determination of HLB values of some nonionic surfactants and their mixtures. *Studia Universitatis Babes-Bolyai Chemia*, 62(4), 451–458.
38. Hong, I. K., Kim, S. I., Lee, S. B. (2018). Effects of HLB value on oil-in-water emulsions: Droplet size, rheological behavior, zeta-potential, and creaming index. *Journal of Industrial and Engineering Chemistry*, 67(3), 123–131.
39. Bureiko, A., Trybala, A., Kovalchuk, N., Starov, V. (2015). Current applications of foams formed from mixed surfactant-polymer solutions. *Advances in Colloid and Interface Science*, 222(1–2), 670–677.
40. Liu, X. C., Zhao, Y. X., Li, Q. X., Niu, J. P. (2016). Surface tension, interfacial tension and emulsification of sodium dodecyl sulfate extended surfactant. *Colloids and Surfaces A: Physicochemical and Engineering Aspects*, 494, 201–208.
41. Yu, X. Y., Miao, X. Y., Li, H., Qiu, K., Zong, R. W. et al. (2022). Influence of seawater on interfacial properties, foam performance and aggregation behaviour of fluorocarbon/hydrocarbon surfactant mixtures. *Journal of Molecular Liquids*, 359(2), 119297.
42. Yan, H. Q., Chen, X. Q., Feng, M. X., Shi, Z. F., Zhang, W. et al. (2019). Entrapment of bacterial cellulose nanocrystals stabilized Pickering emulsions droplets in alginate beads for hydrophobic drug delivery. *Colloids and Surfaces B: Biointerfaces*, 177, 112–120.
43. Mikulcova, V., Bordes, R., Kasparkova, V. (2016). On the preparation and antibacterial activity of emulsions stabilized with nanocellulose particles. *Food Hydrocolloids*, 61, 780–792.
44. Liu, Z., Shen, R., Yang, X. B., Lin, D. H. (2021). Characterization of a novel konjac glucomannan film incorporated with Pickering emulsions: Effect of the emulsion particle sizes. *International Journal of Biological Macromolecules*, 179(2), 377–387.
45. Nesterenko, A., Drelich, A., Lu, H. L., Clause, D., Pezron, I. (2014). Influence of a mixed particle/surfactant emulsifier system on water-in-oil emulsion stability. *Colloids and Surfaces A: Physicochemical and Engineering Aspects*, 457, 49–57.
46. Lu, Y., Wu, H. R., Meng, Z. Y., Jiang, J. T., Jin, Y. et al. (2018). Salt effect on hydrophobically modified polyacrylamide-containing crude oil emulsions: Stability and rheology study. *Colloid and Polymer Science*, 296(3), 515–527.
47. Nowicki, J., Woch, J., Drabik, J., Korasiak, K., Howska, J. et al. (2022). Formation, properties and rheology of paraffin wax oil-in-water emulsions. Stabilizing effect of novel EO/PO/EO block copolymer fatty acid monoesters. *Materials Chemistry and Physics*, 291, 126759.